



OPEN ACCESS

EDITED BY

Sylvain Leduc,
International Institute for Applied
Systems Analysis (IIASA), Austria

REVIEWED BY

Haifeng Liu,
Tianjin University, China
Sudhanya Banerjee,
AspenTech, United States

*CORRESPONDENCE

Xiaoyi Yang,
yangxiaoyi@buaa.edu.cn

SPECIALTY SECTION

This article was submitted to Bioenergy
and Biofuels,
a section of the journal
Frontiers in Energy Research

RECEIVED 15 May 2022

ACCEPTED 11 July 2022

PUBLISHED 17 August 2022

CITATION

Liu Z, Wang Z, Gu X, Liu H, Yang L, Yang J
and Yang X (2022), Intelligent
quantitative assessment on the spray
performance of alternative aviation fuel.
Front. Energy Res. 10:944668.
doi: 10.3389/fenrg.2022.944668

COPYRIGHT

© 2022 Liu, Wang, Gu, Liu, Yang, Yang
and Yang. This is an open-access article
distributed under the terms of the
[Creative Commons Attribution License
\(CC BY\)](https://creativecommons.org/licenses/by/4.0/). The use, distribution or
reproduction in other forums is
permitted, provided the original
author(s) and the copyright owner(s) are
credited and that the original
publication in this journal is cited, in
accordance with accepted academic
practice. No use, distribution or
reproduction is permitted which does
not comply with these terms.

Intelligent quantitative assessment on the spray performance of alternative aviation fuel

Ziyu Liu¹, Zhichao Wang², Xiaoyu Gu², Haobo Liu¹, Luhua Yang¹,
Jingying Yang¹ and Xiaoyi Yang^{2*}

¹School of Aeronautic Science and Engineering, Beihang University, Beijing, China, ²School of Energy and Power Engineering, Energy and Environment International Center, Beihang University, Beijing, China

Drop-in alternative aviation fuel (AAF), as a blend of petroleum-derived kerosene with sustainable jet fuel, has the advantage in CO₂ reduction and could be used without any modifications to the engine and aircraft. Therefore, drop-in AAF blending could not scarify the performance compared to traditional jet fuel. For assessing the spray performance quantitatively, traditional jet fuel (RP-3) with blending alternative compositions including paraffins, cycloparaffins, and aromatics was designed. Carbon number distribution and classification distribution in jet fuel compositions that would influence spray performance are well investigated. The cone angle and liquid length are recognized by a shadow image, while Sauter mean diameter (SMD) and velocity are investigated by phase-Doppler anemometry (PDA). The liquid length and droplet size of bicyclohexane, phenyl-cyclohexane, heptadecane, and octadecane conduct a significant deviation compared with RP-3, which complies with the large deviations of $L_{b(f)} [\sigma^{0.25} \mu_f^{0.25} \rho_f^{0.25}]$, which extracted the fuel property item from the liquid length, and $Oh(f) [\mu_f \sigma^{-0.5} \rho_f^{-0.5}]$, which extracted the fuel property item from the Ohnesorge number. The blending fuels of those cannot be certified as drop-in fuel due to obvious deviation to RP-3, which also presents differences in carbon number distribution and classification distribution. The spray empirical models were established quantitatively to assess the characteristics of the liquid sheet and droplet for discovering the blend fuel effects. The empirical equations of the liquid length and SMD calibrated by evaporation constants can agree well with the experimental data except for blends of bicyclohexane, phenyl-cyclohexane, C17, and C18. The integrated spray performance assessment models developed could benefit from certifying drop-in fuel at the spray level quantitatively.

Abbreviations: RP-3, traditional jet fuel; t_f , liquid sheet thickness; GTL, gas to liquid; FT, Fischer-Tropsch aviation fuel; HRJ, hydrotreated jet fuel; PDA, phase-Doppler anemometry; SMD, Sauter mean diameter; ρ_f , density of the fuel; ρ_g , density of the air; μ_f , fuel dynamic viscosity; Re , Reynolds number; k , evaporation rate constant; \dot{m} , mass flow rate of liquid; θ , spray angle; Oh , Ohnesorge number; $Oh(f)$, fuel characteristic constant of Ohnesorge number; L_b , liquid length; $L_{b(f)}$, fuel characteristic constant of liquid length; d_0 , nozzle exit orifice diameter; We , Weber number; U , total velocity; σ , liquid surface tension; ΔP , injection pressure; evaporation, evaporation constant.

KEYWORDS

alternative fuel, spray characteristics, nozzle, schlieren image, cone angle, liquid length

1 Highlights

- Establishing quantitative spray models based on fuel effects;
- extracting key fuel parameters to certify drop-in fuels at the spray level;
- improving SMD empirical equation by involving evaporation constants; and
- effects of carbon number distribution and classification distribution on spray performance.

2 Introduction

Drop-in AAF could reduce energy consumption and emissions in aviation transportation. Also, it could be used without any modifications to the engine and aircraft. Accordingly, alternative aviation fuel blend as drop-in could not scarify the performance of the engine. Although with the development of alternative fuel refining, more and more refining processes have been certified to blend with traditional jet fuel as drop-in fuel, and the blend ratios should be in compliance with the requirements of ASTM International standards for aviation fuels (Liu et al., 2016). The main reason that the blend ratio should meet the standard is that sustainable jet fuel has different carbon number distribution and classification distribution compared to petroleum-derived kerosene. As the higher blend ratio of sustainable jet fuel could contribute to GHG reduction, the change of carbon number distribution and classification distribution in blend jet fuel should be investigated in detail for coupling engine performance. Few research studies focus on the spray and other related performance for fuel carbon number distribution and classification distribution in jet fuel.

As spray performance is crucial for combustor performance related to engine performance (Chen et al., 2019; Feng et al., 2021), blend effects of alternative aviation fuels have been investigated in the spray performance and the spray model (Sivakumar et al., 2015, 2016). According to atomization mechanisms with a series of empirical models (Rizk and Lefebvre, 1982; Lefebvre, 1987; Wang and Lefebvre, 1987; Chen and Lefebvre, 1994; Lefebvre and Ballal, 2010), spray performances could be influenced by nozzle structure, operation pressure, fuel properties, and environment condition. The fuel properties, including density, viscosity, and surface tension, can significantly influence the droplet size, cone angle, and liquid length. By using a high-speed camera to investigate the spray performance (Monteiro et al., 2009), it is proposed that the surface tension and viscosity could affect the energy transfer process and efficiency and finally lead to

droplet fragmentation and refusion during atomization. The characteristics of cone angle and liquid length were mainly related to density, viscosity, and surface tension, while droplet sizes were determined by the integration of density, viscosity, surface tension, and even evaporability.

The properties of the traditional jet fuels derived from different petroleum industries are quite similar in density, viscosity, and surface tension due to similar feedstock and similar refining processes. However, alternative aviation fuels have obvious differences in compositions even with similar properties due to different feedstock and different refining processes (Yang et al., 2016). For understanding the spray mechanism and predicting the spray performance of alternative aviation fuel blends, Payri et al. (2017) studied the spray characteristics of two gas-to-liquid (GTL) fuels (FT process) in comparison with conventional Jet A-1 fuel under three different pressures. The results demonstrated that the influence of fuel physical properties is insignificant on the spray characteristics at high injection pressures. GTL blend fuels have investigated the spray performance from the view of fuel properties (Kannaiyan and Sadr, 2013; Kannaiyan and sadr, 2014a; Kannaiyan and Sadr, 2014b; Kannaiyan and Sadr, 2014c). They concluded that the lower viscosity and surface tension of blend fuel led to faster disintegration and dispersion than those of Jet A-1 fuel. As the fuel properties of the GTL blend fuel are very similar to traditional jet fuel, spray characteristics of GTL blend fuel can be predicted by empirical relations derived from conventional jet fuels. Sivakumar et al. (2015) investigated the atomization performance of camelina-derived aviation fuel (HRJ process). The results also indicated that the predicted droplet sizes by the empirical model agreed well with experimental droplet sizes for the biofuel spray, while the predicted droplet sizes by the theoretical model presented larger than those of experimental measurement. The empirical models derived from traditional jet fuel can be involved in predicting the spray performance of blend aviation fuel. However, evaporation effects related to environmental factors have not been involved in the equation and result in the limitation of application scenarios (Zhou et al., 2019).

Although the fuel property of blending jet fuel effects on spray performance have been investigated, few research studies have investigated on how the compositions of alternative fuel blends affect spray performance-integrated droplet size, cone angle, and liquid length. As the alternative aviation fuel blend has the advantage in CO₂ reduction, a dataset by blending various individual molecules that might be present in alternative aviation fuels into a conventional aviation fuel has been generated. Traditional jet fuel with blend alternative compositions including paraffins, cycloparaffins, and aromatics was designed

to investigate the spray performance. Spray-related empirical equations have been established for assessing the spray performance quantitatively. The spray performance of fuels (cone angle, liquid length, SMD, and velocity) is fully examined with different carbon number distribution and classification distribution in jet fuel compositions. The integrated spray performance assessment models developed could benefit from certifying drop-in fuel at the spray level quantitatively. The results could contribute to how to use alternative aviation fuels in engines.

3 Methodology

3.1 Composition and property

The compositions in fuels were tested by using a GC-MS system (Agilent 7890A-5975C) with an HP-5 capillary column. The sample was diluted with dichloromethane (1:10, V/V) with the injected volume of 1 μL at the split ratio of 20:1. The oven temperature was set from 40°C to 175°C at 5°C/min and held for 2 min and finally ramped to 320°C at 2°C/min and held for 2 min. The injector and detector temperatures were 280 and 150°C, respectively. The mass spectrometer scan ranged from m/z 30 to m/z 750.

The density (SYA-1884A), the kinematic viscosity (SYD-265H), the surface tension (SFT-A1), and the vapor pressure (MINIVAP VPXpert) were measured with an accuracy of $\pm 0.5 \text{ kg/m}^3$, $\pm 0.3\%$, $\pm 0.1\%$, and 0.1 Kpa, respectively.

For comparison with the effects of carbon number distribution and classification distribution, 14 typical hydrocarbon compositions are extracted from alternative aviation fuel to blend with jet fuel to investigate the spray performance. From the view of carbon number, paraffins, including tridecane (C13), tetradecane (C14), pentadecane (C15), cetane (C16), heptadecane (C17), and octadecane (C18), were blended with jet fuel (10%, weight), respectively. From the view of classification, n-paraffin (n-dodecane C12), iso-paraffin (iso-dodecane iso-C12), cycloparaffins (ethyl-cyclohexane C8, butyl-cyclohexane C10, and bicyclohexane C12), and aromatics (ethyl-benzene C8, butyl-benzene C10, and phenyl-cyclohexane C12) were blended with jet fuel (10%, weight), respectively.

3.2 Spray measurement

Spray measurements are divided into photography and non-photography methods. The photography method explores the required information of cone angle and liquid length by taking pictures of the spray field and then processing the obtained photos. Non-photography uses a laser as the incident light source

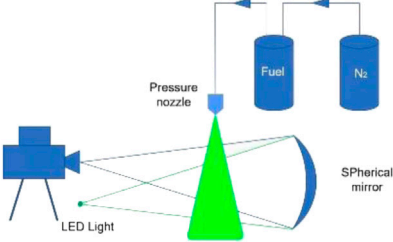
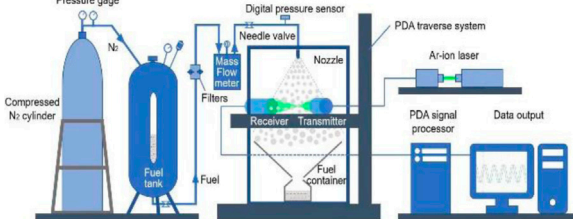
to test the SMD and velocity of droplets by phase-Doppler anemometry (PDA), as shown in Table 1.

As the swirl nozzle has been widely used to assess the spray performance because it has the ability to atomize the fuel in the ambient atmosphere and it is available to reflect the influence of different fuel properties on the atomization performance, a swirl nozzle with a 100- μm exit diameter has been involved in the spray test. A spray rig includes a nitrogen cylinder, a fuel storage tank, a swirl nozzle, and a set of filters installed in the flow fuel line. A digital pressure sensor and a mass flow meter were placed upstream of the nozzle to measure the injection pressure and the mass flow rate of the spray.

For shadow measurement, the shadow system includes xenon LED lights, concave mirrors, and high-speed cameras. The shadow device consisted of a T6 LED point light source with a luminous flux of 1,000 LM. The spherical mirror has a diameter of 203 mm and a focal length of 800 mm to form the reflective light path and illuminate the spray environment. The principal measurement of this technique is based on the deflection of a collimated light beam crossing gradients of the index of reflection in a transparent medium. The atomizing nozzle is placed between the concave mirror and the camera. After the light is reflected through the atomizing field by the concave mirror, the images with spray information focus on the camera, thus obtaining the image of the fuel atomizing field with atomizing performance information. An iron ball was used as a reference to calibrate the length. The atomized images at the nozzle outlet were investigated to analyze the cone angle and liquid length. The atomized images were conducted by the Pillow module in Python to extract the data information. The rectangle fields with the nozzle outlet as the center line (pixel 197×105) were converted into a grayscale with a range of 0–255. As the grayscale value is related to the LED light intensity, the mean value of the maximum and minimum grayscale values is selected as the threshold of the identification boundary. The grayscale values of pixel points were investigated from vertical direction and horizontal direction successively.

For the PDA test, the PDA experimental system (Dantec, BSA P60) consists of an argon particle laser generator, laser transmitter, laser receiver, data output, and signal processor. It could provide measurements for particle size, droplet velocity, and concentration along the spatial distribution in the spray field. Each measurement point in the spray field is set to collect 6,000 effective droplets or 15 s duration in order to reduce the measurement error. From the view of the accuracy of PDA, the particle size is 0.5–1,000 μm with an accuracy of 95–97%, while the maximum velocity of 500 m/s can be investigated with the accuracy of 99.8%. Table 1 shows the measurement points in the PDA experiment. The measuring set started at 1 mm downstream from the nozzle exit, and the measuring points were arranged along Z and X.

TABLE 1 Evaluation of the spray performance.

	Shadow method	PDA method
Test rig		
Instrument	Xenon LED lights, concave mirrors, and high-speed cameras	PDA Dantec, BSA P60
Method	Extract the image data information (cone angle and liquid length) by Pillow module in Python (the detail in Supplement material)	Measurement points (SMD and velocity) started at 1 mm downstream from the nozzle exit and measuring points arranged along Z and X (the detail in the previous article (Zhou et al., 2019))

4 Results and discussion

4.1 Compositions and properties

The compositions in traditional jet fuel (RP-3) can be classified as classification distribution and carbon number distribution, as given in Figure 1. The carbon distributions of both RP-3-1 and RP-3-2 display a normal distribution from C7 to C19 centered on C10, C11, and C12. The carbon number distribution and classification distribution in traditional jet fuel and blend fuels are shown in Figure 1B. For blend fuel including paraffins (C12–C14), cycloparaffins (C8, C10, C12), or aromatics (C8, C10, C12) in jet fuel (RP-3), carbon number distribution can keep a normal distribution centered on C10, C11, and C12 except when blending the paraffins (C15–C18). In comparison with RP-3 in classification, the blend of phenyl-cyclohexane (C12) conducts obviously different in cyclo-aromatic concentration, while the blend of bicyclohexane leads to the higher concentration in di&tri-cycloparaffins, as shown in Figure 1A. In addition, the blends of ethyl-cyclohexane and butyl-cyclohexane contribute to the higher concentration of cycloparaffins.

The obvious changes in carbon number distribution and classification distribution result in the fuel property change. The key properties of jet fuels were related to the spray performance including density, viscosity, surface tension, and vapor pressure, as given in Figure 2. Viscosity and vapor pressure are more sensitive than density and surface tension. In respect of density and surface tension, the variations keep in the range of $\pm 3\%$, while viscosity can get to 11.5% (bicyclohexane) and vapor pressure gets to 17.2% (ethyl-cyclohexane). The vapor pressure of blending jet fuel decreased significantly except for ethyl-benzene (C8) and ethyl-cyclohexane (C8), while the viscosity of blending jet fuel increased significantly except for ethyl-benzene and ethyl-cyclohexane. The results indicated that

the blend of C8–C18 mainly contributes to the change of jet fuel in vapor pressure and viscosity. $L_{b(f)} [\sigma^{0.25} \mu_f^{0.25} \rho_f^{0.25}]$ is a characteristic constant that is extracted from the fuel property item from the liquid length and defined as the characteristic constants of liquid length. $Oh_{(f)}$ is defined as $[\mu_f \sigma^{-0.5} \rho_f^{0.5}]$ that is extracted from the fuel property item from the Ohnesorge number. Those characteristic constants' effects on spray performance are in Sections 3.2 and 3.4.

4.2 Recognition of the cone angle and liquid length

Fuels were accelerated to rotate at high speed in the nozzle by pressure drop and form a liquid film in the convergent cavity. The liquid film appeared continuously at the nozzle outlet and was sheared and broken by the aerodynamic force along the downstream of the nozzle. When the liquid filament appears no longer continuously, the grayscale value in the image takes a jump. The jump of grayscale values as a two-dimensional array is defined as the left boundary point and the right boundary point along the horizontal direction, respectively. Two boundary lines can be drawn along the vertical direction based on the left boundary points and the right boundary points. The cone angle can be obtained according to the geometrical relationship of two boundary lines. Along the horizontal direction, the jump of grayscale values is defined as the boundary point of liquid length. The boundary points of liquid filaments are discontinuous at different positions due to non-steady flow, as given in Supplementary Figure S3, and accordingly, the length of liquid filaments was integrated and evaluated by using arithmetic mean with 50 images.

The coordinate of each pixel point was set as 1, and the grayscale values were extracted far from the nozzle at 10 pixels, 20 pixels, 30 pixels, 40 pixels, and 50 pixels, respectively. All

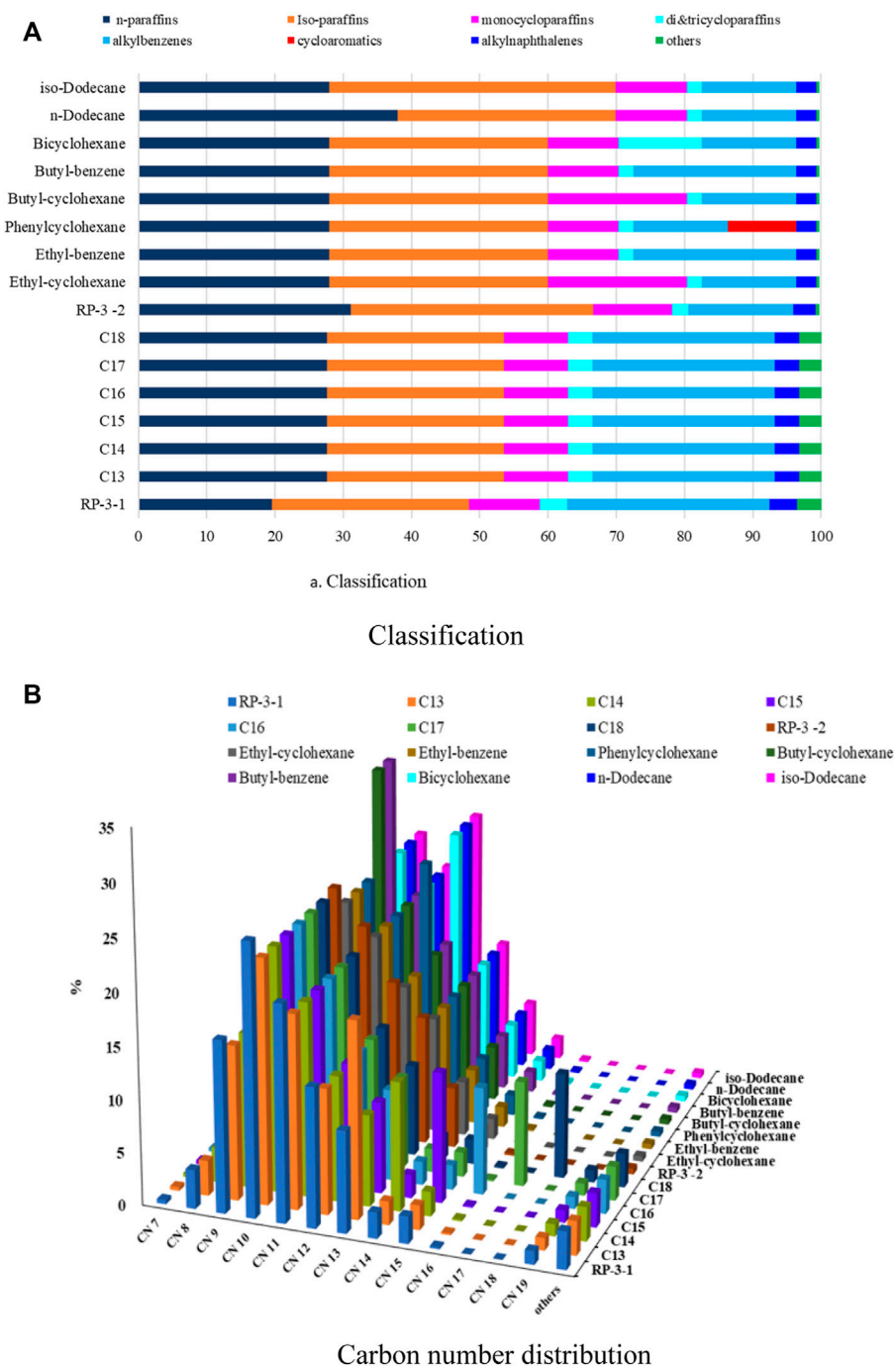


FIGURE 1 Carbon number distribution and classification of blending fuels. (A) Classification; (B) carbon number distribution.

image grayscale values were distributed between 30 and 220. Taking half pixel point as the error on the scale, the boundary point identification error is $\Delta x \leq 0.5$, and thus, the cone angle error was expressed as follows:

$$\Delta\theta = \arcsin \frac{\Delta x}{l} \approx \frac{\Delta x}{l} \leq \frac{0.5}{50} = 0.01 \text{ (Radians)}.$$

By the same way, the relative error of liquid film length within 1% was expressed as follows:

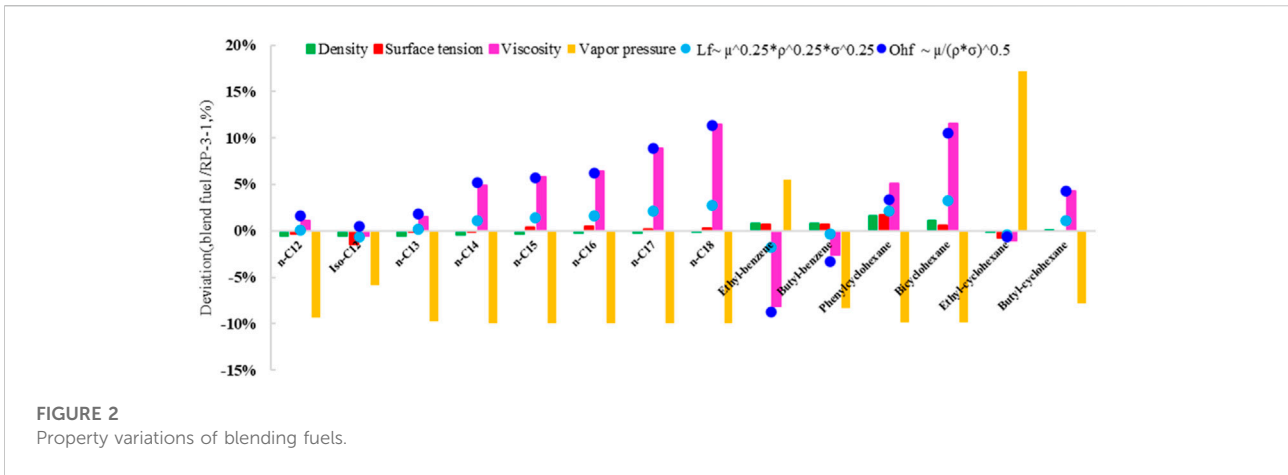


FIGURE 2 Property variations of blending fuels.

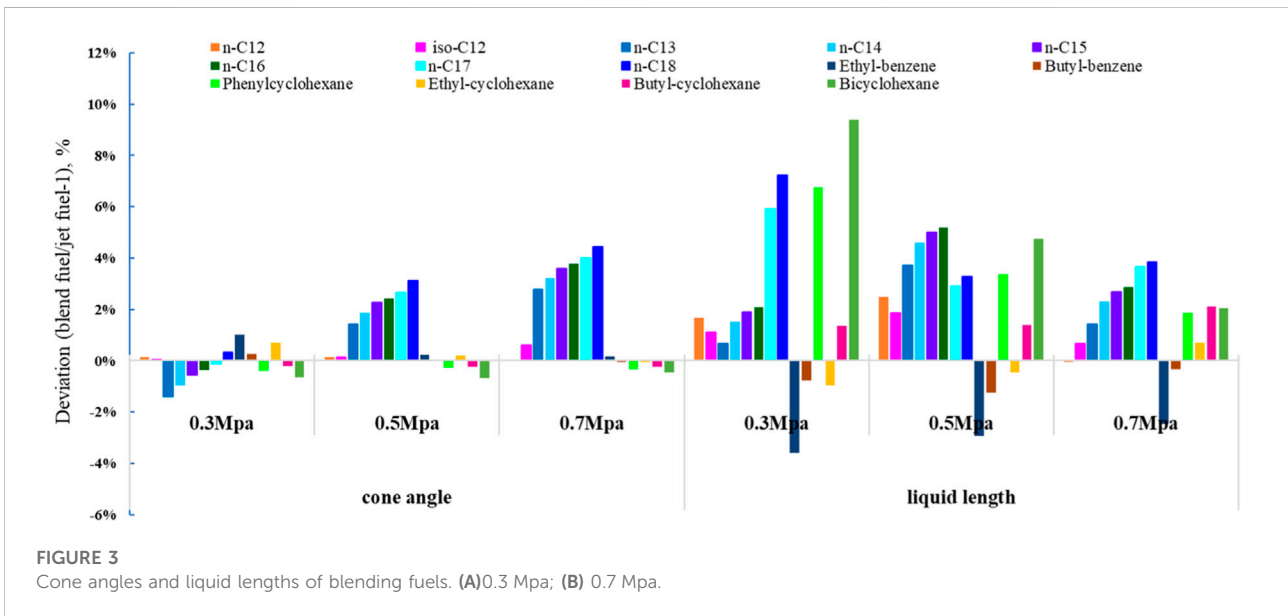


FIGURE 3 Cone angles and liquid lengths of blending fuels. (A) 0.3 Mpa; (B) 0.7 Mpa.

$$\frac{\Delta l}{l} \leq \frac{0.5}{50} = 1\%.$$

For all blending jet fuels, the cone angles broadened, while the liquid length shortened with the increase of pressure, as given in Figure 3, which is coincident with the characteristics of the swirl nozzle. However, the variations of blending fuels performed differently due to property differences in comparison with RP-3 jet fuel.

The cone angles of paraffins changed obviously in comparison with cycloparaffins and aromatics at higher pressures. However, the variations of cone angles of 14 blending jet fuels were limited to the range of -1.4 to 4.42%, which indicated that the deviation of fuel properties contributes less to the variations of cone angles. The results are coincident with the characteristics of the swirl nozzle, which is

that the cone angle is mainly affected by the geometric characteristics of the nozzle. However, the liquid length of 14 blending jet fuels varies obviously. The liquid lengths of blend fuel including bicyclohexane, phenyl-cyclohexane, C17, and C18 extended at different pressures and appeared obviously, especially in low pressure. In comparison with properties, both bicyclohexane and phenyl-cyclohexane present a positive deviation in density, viscosity, and surface tension, while C17 and C18 present a larger deviation in viscosity. In comparison with the characteristic constants of liquid length, $L_{b(f)}$ and $Oh_{(f)}$ all present a larger positive deviation from RP-3. The liquid lengths of ethyl-benzene and butyl-benzene decreased at various pressures and therein ethyl-benzene dropped significantly. Those characteristic constants of $L_{b(f)}$ and $Oh_{(f)}$ are characterized by negative deviation. The results indicated that a large deviation of $L_{b(f)}$ and $Oh_{(f)}$ could lead to a large deviation of liquid length compared with

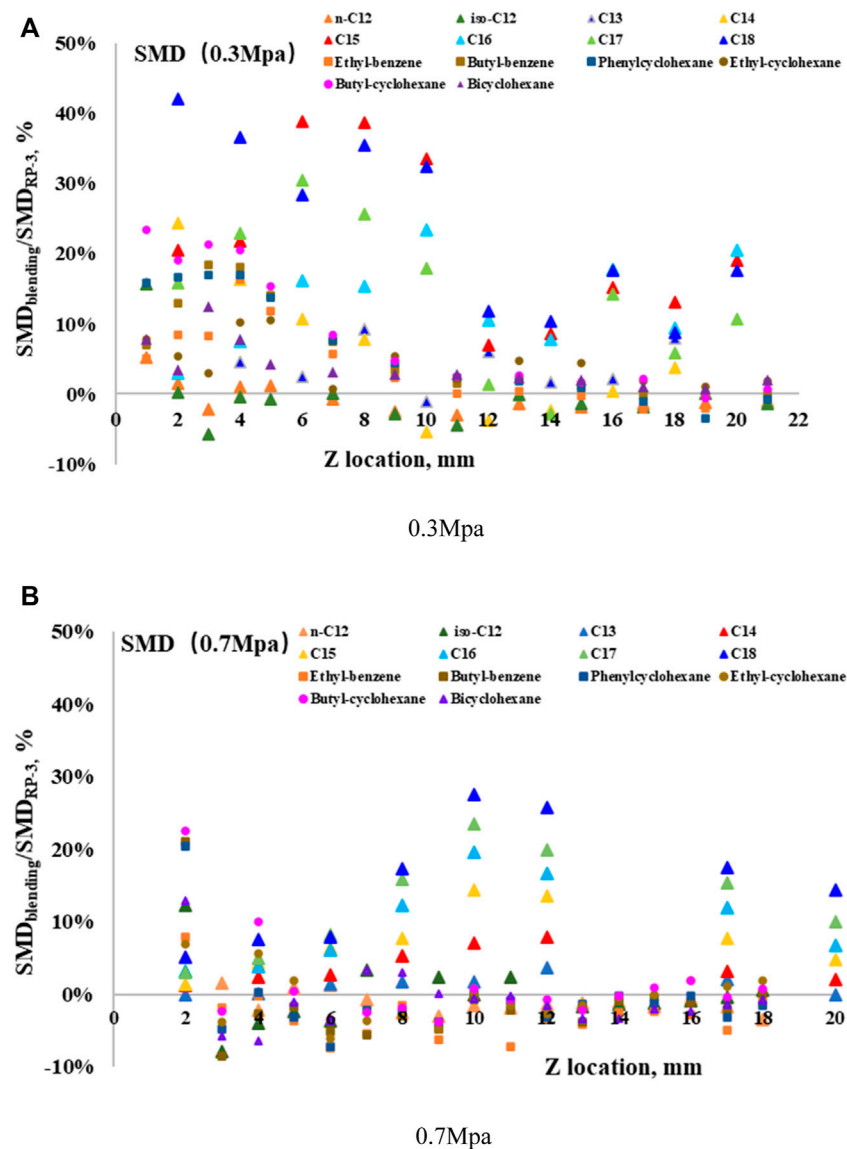


FIGURE 4
SMD distribution of blending fuel in comparison with RP-3. (A) 0.3 Mpa; (B) 0.7 Mpa.

RP-3. $Oh_{(t)}$ is positively associated with the liquid length. The detailed mechanism is in Section 3.4.2.

4.3 Droplet size and velocity

The droplet size and velocity control the combustion performance. The flame stabilization requires that the velocity is matched to the burning velocity of the flame base. The bigger droplet size could lead to soot in the combustor. These have been investigated from the view of carbon number distribution and classification distribution in jet fuel compositions.

The spray field was classified into the liquid sheet zone (primary spray zone) and the droplet zone (secondary spray zone). Along the axial direction (Z) and radial direction (X) from the nozzle exit, SMD distribution of blending fuel in comparison with RP-3 is shown in Figure 4. In the primary spray zone, droplets were investigated in the liquid sheet zone, which indicated few droplets splashed from the liquid sheet due to aerodynamic force. The significant difference in the axial SMD appears in the liquid sheet zone ($z < 2$ mm) and droplet zone in $2 \text{ mm} < Z < 5$ mm compared with RP-3. On the one hand, the difference was attributed to the fact that the interfaces of blending fuels between the liquid sheet zone and droplet zone are located in different positions. On the other hand, the difference in the

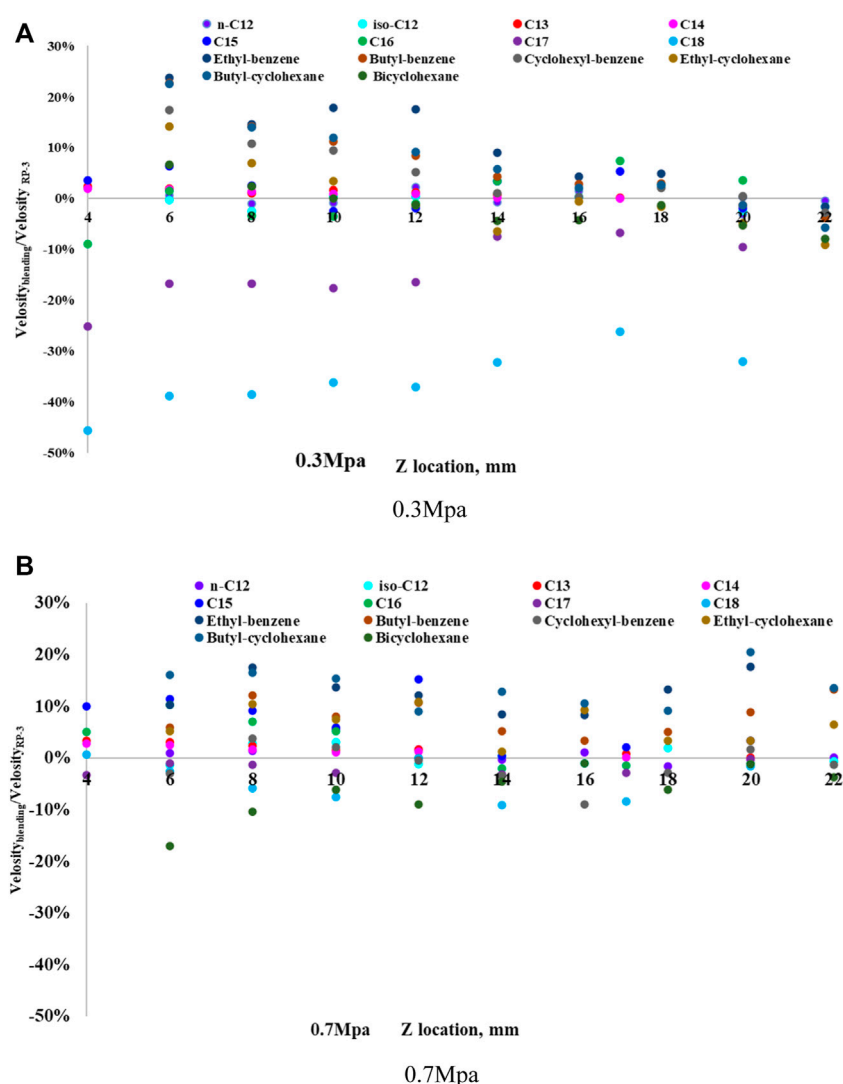


FIGURE 5
Velocity distribution of blending fuel in comparison with RP-3. (A) 0.3 Mpa; (B) 0.7 Mpa.

thickness and velocity of liquid films results in differences in splashed droplets. Although splashing droplets derived from liquid sheets are random due to instability flow, the obvious enlargement of droplet size is presented in C15, C16, C17, C18, bicyclohexane, and phenyl-cyclohexane despite being at low pressure or high pressure. The results indicated that the compounds with larger space structures could amplify droplet size in the liquid film zone and at the interfaces between liquid sheet zones.

In the droplet zone, droplet breakup, droplet evaporation, and droplet-to-droplet collisions were integrated together to influence the size and velocity of the droplet. From the view of fuel classification, the droplet sizes of aromatics and cycloparaffins blending performed scarcely different in the droplet zone, while those of paraffins (C15, C16, C17, and C18) performed significantly different in both the liquid sheet zone and droplet zone. The axial SMD profiles of

aromatics and cycloparaffins were almost as same as RP-3 at 0.7 Mpa, which means that when the blending ratio was below 10%, the effect of blending on spray droplet size was mainly reflected at the low pressure. From the view of carbon number distribution, the increase in the carbon number prevents the droplet from breaking. The increase in the carbon number beyond the range of C16 could lead to an obvious deviation from traditional jet fuel. The larger droplet size could be induced by larger viscosity coupling with lower evaporability. A significant rise of larger diameter droplets at farther locations from the atomizer exit may be a result of the combined effect of fuel evaporation and droplet-to-droplet collisions.

The velocity distribution of blending fuel in comparison with RP-3 is shown in Figure 5. In the liquid sheet zone, the ambient air was dragged into the spray cone, which resulted in the drop of velocity. The droplets in the spray periphery and intermediate region were

unstable, and the bigger droplets usually kept a higher moment in the periphery region, while small droplets maintained lower velocity in the intermediate region. By comparing the axial distribution of mean radial velocity, the obvious variation is present at the position close to the nozzle exit as the SMD profile. The droplets splashed from the liquid sheet into the spray periphery and intermediate regions, and those droplet velocities were lower than the evolution of the liquid sheet with random direction.

In the droplet zone, the axial decay rates of the droplet velocity of blending fuel became similar and got close to the droplet velocity of RP-3 at Z = 16 mm at 0.3 Mpa while at Z = 17 mm at 0.7 Mpa. The droplet velocity presents a significant difference at the area of Z < 15 mm at 0.3 Mpa. C15, C16, C17, and C18 blending fuels had lower droplet velocities while ethyl-benzene, butyl-benzene, cyclohexyl-benzene, ethyl-cyclohexane, and butyl-cyclohexane had a higher droplet velocity than with RP-3 at 0.3 Mpa. C16, C17, and C18 performed significantly different than RP-3 even at 0.7 Mpa, while the other fuels tend to have an RP-3 velocity profile.

In respect of classification distribution of fuel on droplet velocity, the droplet velocities of n-dodecane (C12) and iso-dodecane (C12) mixtures were very close to RP-3, regardless of different pressures compared to bicyclohexane (C12) and phenyl-cyclohexane (C12) mixtures. In respect of carbon number distribution, it could be clearly observed that the droplet size and droplet velocity of paraffins (C12-C14) are almost as same as those of RP-3 both in the liquid sheet zone and in the droplet zone. However, C15-C18 performed obviously different in droplet size and droplet velocity, regardless of in the liquid sheet zone and in the droplet zone compared with RP-3. Aromatic blending presented a higher velocity due to lower viscosity. n-dodecane and iso-dodecane present similar physical properties which led to similar spray characteristics. By comparing the effects of fuel classification distribution with carbon number distribution on velocity, higher carbon numbers with larger special structures influenced droplet velocity significantly.

4.4 Assessment model of spray performance

4.4.1 Cone angle predicting model

Assessment of the performance of alternative aviation fuel should couple with the liquid sheet characteristics and droplet characteristics.

The mass flow can be fitted by test results coupling with the nozzle geometrical parameter (Rizk and Lefebvre, 1985), flow conditions, and fuel properties, as follows:

$$m = \dot{m}_f = C_d A_n \sqrt{2\rho_f \Delta P_f} = A \mu_f \sqrt{2\rho_f \Delta P_f}.$$

\dot{m}_f is the mass flow rate of fuels measured at different injection pressures (kg/s); ΔP_f is the injection pressure in the experiment (Pa); ρ_f is the density of fuel (kg/m³), and μ_f is the liquid

dynamic viscosity (kg/(ms)); A is a constant related with the structure of nozzle.

A relation for the estimation of liquid sheet thickness ρ_f in a simple swirl nozzle is proposed by Rizk and Lefebvre (1985).

$$\begin{aligned} t_f &= 3.66 \left(\frac{m d_0 \mu_f}{\rho_f \Delta P} \right)^{0.25} = 3.66 d_0^{0.25} \left(\frac{\mu_f}{\rho_f \Delta P} \right)^{0.25} m^{0.25} \\ &= 3.66 A^{0.25} d_0^{0.25} \left(\frac{\mu_f}{\rho_f \Delta P} \right)^{0.25} (\rho_f \Delta P_f)^{0.125} \\ &= 3.66 A^{0.25} d_0^{0.25} \Delta P_f^{-0.125} \mu_f^{0.5} \rho_f^{-0.125}, \end{aligned}$$

where d_0 is the radius of the nozzle exit; ρ_a is the density of ambient air (kg/m³).

We_l is characterized by the ratio of aerodynamic force to surface tension, which can be further expressed as the following by integrating with liquid sheet thickness:

$$\begin{aligned} We_l &= \frac{\rho_f v^2 t_f}{\sigma} = \frac{\rho_f}{\sigma} \frac{2 \Delta P_l}{P_f} 3.66 \left(\frac{m d_0 \mu_f}{\rho_f \Delta P} \right)^{0.25} = \frac{\rho_f}{\sigma} \frac{2 \Delta P_l}{P_f} 3.66 \left(\frac{d_0 \mu_f}{\rho_f \Delta P} \right)^{0.25} m^{0.25} \\ &= 3.66 * \sqrt{2} A^{0.25} d_0^{0.25} \sqrt{2} \frac{\rho_f}{\sigma} \frac{2 \Delta P_l}{P_f} \left(\frac{\mu_f}{\rho_f \Delta P} \right)^{0.25} \mu_f^{0.25} (\rho_f \Delta P_f)^{0.125} \\ &= [7.32 A^{0.25} d_0^{0.25}] [\Delta P_f^{0.875}] [\sigma^{-1} \mu_f^{0.25} \rho_f^{-0.125}] \\ &= [structure(A, d_0)] [condition(\Delta P_f)] [fuel(\sigma, \mu_f, \rho_f)]. \end{aligned}$$

By further mathematics deformation to extract the fuel effect, three square brackets present structure effects, operation effects, and fuel effects. For cone angle, according to Kim et al. (2007), the atomization cone angle can be expressed by the relation of the We_l number of the axial atomization of fuel, which indicated that fuel effects are attributed to the integration of surface tension, viscosity, and density.

$$\begin{aligned} \frac{\theta}{\theta_o(z)} &= 0.56 We_l^{0.12} \\ &= [structure(Ad_0)] [condition(\Delta P_f)] [fuel(\sigma, \mu_f, \rho_f)]. \end{aligned}$$

However, according to Lefebvre (Rizk and Lefebvre, 1985), the cone angle can be expressed based on the swirl nozzle structure:

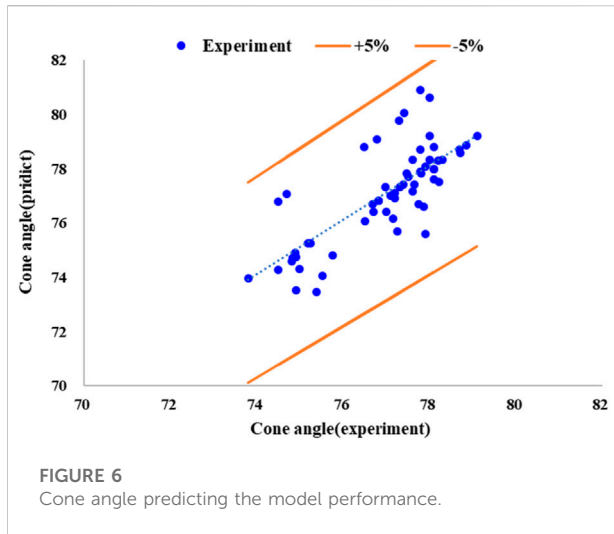
$$\theta = 6 \left(\frac{D_s d_0}{A_p} \right)^{0.15} \left(\frac{\Delta P_f d_0^2 P_f}{\mu_f^2} \right)^{0.11},$$

where A_p is the total inlet port area; D_s is the swirl chamber diameter;

By further mathematical deformation, then

$$\begin{aligned} \theta &= \left[6 \left(\frac{D_s d_0}{A_p} \right)^{0.15} d_0^{20.11} \right] [\Delta P_f^{0.11}] \left[\left(\frac{\rho_f}{\mu_f} \right)^{0.11} \right] \\ &= [structure(D_s, A_p d_0)] [condition(\Delta P_f)] [fuel(\mu_f, \rho_f)]. \end{aligned}$$

The equation of Lefebvre indicated that fuel effects depend mainly on viscosity and density. These different mathematical



equations indicated the different broken mechanisms, which maybe attributed to the different atomizer structures and environmental conditions.

The following cone angle equation can be expressed based on the swirl atomizer geometrical parameter:

$$\cos^2 \frac{\theta}{2} = \frac{1-x}{1+x},$$

$$\text{where } X = (d_0 - 2t_f)^2 / d_0^2.$$

$\cos \frac{\theta}{2}$ can be further expressed by integrating with liquid sheet thickness:

$$\cos \frac{\theta}{2} = [\text{structure}(A, d_0)] [\text{operation}(\Delta P_f)] [\text{fuel}(\mu_f \rho_f)].$$

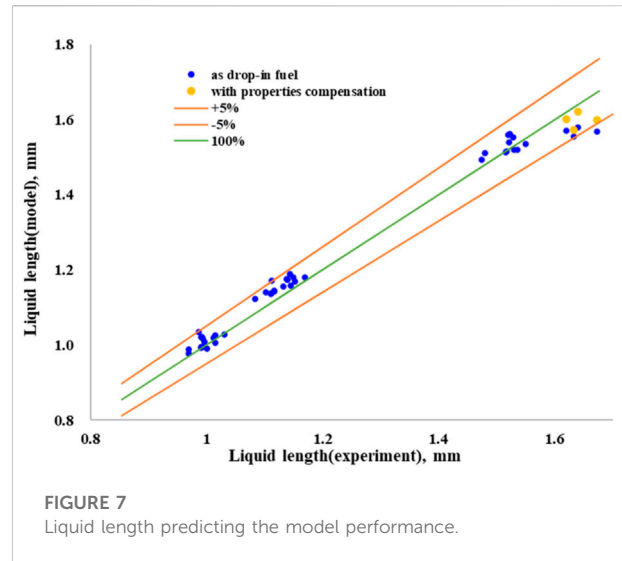
In compliance with the experimental results, a modified empirical relation on the spray cone angle of spray liquid sheets has been fitted and expressed as

$$\cos \frac{\theta}{2} = K [P^{-0.025}] [\rho^{-1} \mu^{-0.05}].$$

All of the test data were distributed within an error range of 5%, which suggested that the developed empirical formula had a high accuracy in estimating the spray cone angle of blending fuels. The comparison between experimental results and the empirical equation results is shown in Figure 6. From the developed empirical formula, the cone angle mainly depends on fuel properties (density and viscosity) and pressure. The results indicated that surface tension had little influence on the cone angle for a swirl atomizer.

4.4.2 Liquid length predicting model

According to Kim et al. (2007), the dimensionless liquid film length model can be expressed as:



$$L_b(\text{KIM}) = C \cdot t_f \left(\frac{\rho_g}{\rho_f} \right)^{-1} We_l^{-0.5}.$$

According to Rizk and Lefebvre (1985), the liquid film length is expressed as

$$L_b(\text{Lefebvre}) = 0.123 t_f^{0.5} We^{-0.5} Re^{0.6}.$$

By further mathematical deformation, then

$$L_b(\text{KIM}) = C \cdot t_f \left(\frac{\rho_g}{\rho_f} \right)^{-1} We_l^{-0.5} = A [P^{-0.5625}] [\rho_g^{-1} \sigma^{0.5} \rho_l^{0.4375} \mu_f^{0.25}],$$

$$L_b(\text{Lefebvre}) = 0.123 t_f^{0.5} \left(\frac{\rho_f v^2 t_f}{\sigma} \right)^{-0.5} \left(\frac{\rho dv}{\mu} \right)^{0.6} = A [\Delta P_f^{-0.2}] [\sigma^{0.5} \mu_f^{-0.6} \rho_f^{0.3}].$$

Integrated with Rizk and Lefebvre (1985) and Kim et al. (2007), the liquid length is related to We, Re, t_f , ρ_f , and ρ_g .

4.4.3 The liquid length can be expressed as

$$L_b = We^{n^*} Re^{m^*} t_f^{i^*} \left(\frac{\rho_l}{\rho_g} \right)^j.$$

Assuming ρ_g as a constant, by fitting the test results at various pressures, the liquid length empirical equation including traditional jet fuel can be obtained as

$$L_b(\text{drop-in jet fuel}) = A [\Delta P_f^{-0.5}] [\sigma^{0.25} \mu_f^{0.25} \rho_f^{0.25}].$$

Except for bicyclohexane and phenyl-cyclohexane, all blend fuels conducted the same mechanism as traditional jet fuel. However, both bicyclohexane and phenyl-cyclohexane present all positive deviation in density, viscosity, and surface tension

when compared with jet fuel, which cannot match this mechanism and is out of the range of $\pm 5\%$.

Oh is defined as $Oh = \frac{\mu_f}{\sqrt{\rho_a d}} = \frac{\sqrt{We}}{Re} = \frac{\text{Viscous forces}}{\sqrt{\text{inertia} \cdot \text{surface tension}}}$, which indicated a contrast of forces. Blend fuels with high deviation in density, viscosity, and surface tension cannot be considered as the drop-in jet fuel as RP-3, which indicated that the breakup mechanism changed. According to experimental results by property compensation, those blend fuels complied with the liquid length empirical equation as the following:

$$L_b \text{ (non-drop-in jet fuel)} = A [\Delta P_f^{-0.5}] [\sigma^{0.5} \mu_f^{0.5} \rho_f^{0.5}].$$

The liquid length empirical equation with property compensation could achieve a good fit for the test data with a deviation range below 5% shown in Figure 7. In spite of the liquid length empirical equation derived from drop-in fuel or non-drop-in jet fuel, the fuel with higher surface tension, viscosity, and density was more likely to produce a longer liquid length.

4.4.3 Sauter mean diameter predicting model

Rizk and Lefebvre established the empirical model of atomized droplet SMD as

$$SMD = \sigma^{0.25} \mu_f^{0.25} \dot{m}_f^{0.25} \Delta P_f^{-0.5} \rho_A^{-0.25}.$$

The empirical models of atomizing the droplet size for the swirl nozzle were used to express as follows:

$$SMD = K \sigma^a \mu_f^b \dot{m}_f^c \Delta P_f^d \rho_g^f.$$

However, the evaporation effect related to the environmental factor has not been involved in the equation and results in the limitation of application scenarios. According to the evaporation law, SMD₀ of the droplet size at the initial time changes to SMD_t of the droplet size at t time.

$$SMD_0^2 - SMD_t^2 = kt,$$

where k is the evaporation rate constant and t is the time, which depended on the droplet process exiting from the nozzle orifice and changes with time, temperature, pressure, and droplet composition. Assuming $k t = K_{\text{evaporation}}$ (constant) at certain blending fuel at the same environmental condition, $K_{\text{evaporation}}$ is defined as the evaporation constant which is related to boiling point and vapor pressure. Hence, the SMD of the empirical model can be modified with $K_{\text{evaporation}}$:

$$SMD^2 = (2.25 P^{-0.5} \sigma^{0.25} \mu_f^{0.25} \dot{m}_f^{0.25} \rho_f^{-1.5} \rho_a^{-0.25})^2 + K_{\text{evaporation}}.$$

The evaporation constant $K_{\text{evaporation}}$ was caused by high relative velocities between the droplet and the surrounding gas and resulted in fast evaporation, especially in light components with higher vapor pressure and lower boiling point in blending fuels. This empirical formula combined interaction between the physical properties of

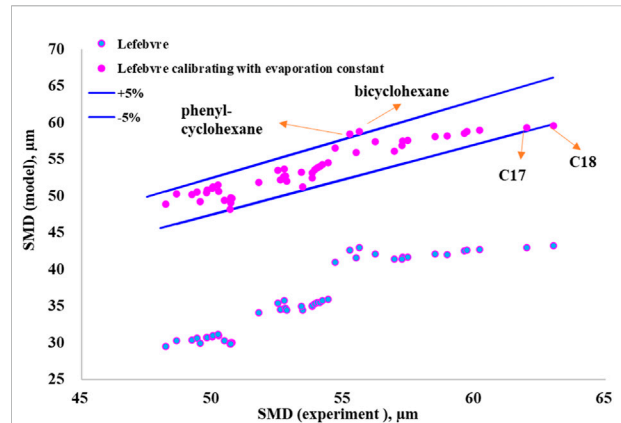


FIGURE 8 SMD predicting the model performance.

fuels with experimental condition differences. The evaporation equilibrium took place following the fuel spray process, and a change in the spatial droplet composition occurred. However, the evaporation equilibrium is closely related to environmental temperature and humidity and conducts differently in the closed space or in the open space, which leads to different diffusion resistance mechanisms in evaporation. As SMD distribution is coupled with the effects of evaporation, it should be controlled by the deviation of the boiling point and vapor pressure. By mathematics fitting, based on test data coupling boiling point, $K_{\text{evaporation}}$ can be expressed as follows:

$$K_{\text{evaporation}} = 285.95 \ln(T_{bp}) + 38.381,$$

where T_{bp} is the boiling point of additive compositions, and P is the vapor pressure of additive compositions.

From Figure 8, SMD calibrated by evaporation constants can agree well with the experimental data. As the experiment was conducted by the same nozzle at the same environmental condition, the deviations are attributed to the fuel effects. Except for bicyclohexane, phenyl-cyclohexane, C17, and C18, all blend fuels complied with the SMD empirical equation, which indicated the same mechanism as traditional jet fuel. From the view of liquid length, both bicyclohexane and phenyl-cyclohexane cannot match the mechanism of traditional jet fuel. In respect of SMD, blend fuels of bicyclohexane, phenyl-cyclohexane, C17, and C18 cannot be certified as drop-in fuels due to obvious deviation, which also present deviation in carbon number distribution and classification distribution.

5 Conclusion

In this study, to investigate the effects of alternative components, drop-in AAF blending with traditional jet fuel on spray performance is well investigated. The obvious changes in carbon number

distribution and classification distribution result in the fuel property change. Viscosity and vapor pressure are more sensitive than density and surface tension. The deviation of fuel properties contributes less to the variations of cone angles. However, the liquid length of bicyclohexane, phenyl-cyclohexane, C17, and C18 increased obviously at various pressures. Moreover, those performed obviously different in droplet size and droplet velocity compared to RP-3 both in the liquid sheet zone and in the droplet zone. The higher carbon number with a larger special structure influenced spray performance significantly. The SMD empirical equation can be performed within an error range of 5% by involving the evaporation constant. The developed empirical equation including cone angle, liquid length, and SMD can match well with traditional jet fuel, which can contribute to certifying the drop-in fuel in the spray level. The large deviation of $L_{b(t)}$ and $Oh_{(t)}$ could lead to a large change in spray performance compared with RP-3.

Data availability statement

The original contributions presented in the study are included in the article/Supplementary Material; further inquiries can be directed to the corresponding author.

Author contributions

All authors listed have made a substantial, direct, and intellectual contribution to the work and approved it for publication.

References

- Chen, B., Feng, L., Wang, Y., Ma, T., Liu, H., Geng, C., et al. (2019). Spray and flame characteristics of wall-impinging diesel fuel spray at different wall temperatures and ambient pressures in a constant volume combustion vessel. *Fuel* 235, 416–425. doi:10.1016/j.fuel.2018.07.154
- Chen, S. K., and Lefebvre, A. H. (1994). Spray cone angles of effervescent atomizers. *At. Spr.* 4, 291–301. doi:10.1615/atomizspr.v4.i3.40
- Feng, L., Sun, X., Pan, X., Yi, W., Yao, M., Wang, Y., et al. (2021). Gasoline spray characteristics using a high pressure common rail diesel injection system by the method of laser induced exciplex fluorescence. *Fuel* 302 (3), 121174. doi:10.1016/j.fuel.2021.121174
- Kannaiyan, K., and Sadr, R. (2014a). Effect of fuel properties on spray characteristics of alternative jet fuels using global sizing velocimetry. *At. Spr.* 24, 575–597. doi:10.1615/AtomizSpr.2014008620
- Kannaiyan, K., and Sadr, R. (2014b). Experimental investigation of spray characteristics of alternative aviation fuels. *Energy Convers. Manag.* 88, 1060–1069. doi:10.1016/j.enconman.2014.09.037
- Kannaiyan, K., and Sadr, R. (2014c). Experimental study of the effect of fuel properties on spray performance of alternative jet fuel. *ASME Turbo Expo/Turbine Tech. Conf. Expo.* doi:10.1115/GT2014-25842
- Kannaiyan, K., and Sadr, R. (2013). Spray characteristics of fischer-tropsch alternate jet fuels. Proceedings of the ASME Turbo Expo 2013: Turbine Technical Conference and Exposition. Volume 2: Aircraft Engine; Coal, Biomass and Alternative Fuels; Cycle Innovations. doi:10.1115/GT2013-95761
- Kim, D., Im, J.-H., Koh, H., and Yoon, Y. (2007). Effect of ambient gas density on spray characteristics of swirling liquid sheets. *J. Propuls. Power* 23, 603–611. doi:10.2514/1.20161
- Lefebvre, A. H., and Ballal, D. R. (2010). *Gas turbine combustion*. Boca Raton, FL: CRC Press. doi:10.1201/9781420086058
- Lefebvre, A. H. (1987). The prediction of Sauter mean diameter for simplex pressure-swirl atomizers. *At. Spray. Technol.* 3, 37–51.
- Liu, Z., Yang, X., and Ding, S. (2016). Assessment the safety of alternative aviation fuels in aero-engine. *Proc. ASME 2016 Power Conf.* 2016, 59520. doi:10.1115/POWER2016-59520
- Monteiro, J. P., Rasteiro, M. G., and Barata, J. M. M. (2009). An experimental investigation on the relative roles of energy input, surface tension, and viscosity on the breakup of a liquid drop. *At. Spr.* 19, 1193–1207. doi:10.1615/AtomizSpr.v19.i12.70
- Payri, R., Viera, J. P., Gopalakrishnan, V., and Szymkowitz, P. G. (2017). The effect of nozzle geometry over the evaporative spray formation for three different fuels. *Fuel* 188, 645–660. doi:10.1016/j.fuel.2016.10.064
- Rizk, N. K., and Lefebvre, A. H. (1985). Internal flow characteristics of simplex swirl atomizers. *J. Propuls. Power* 1, 193–199. doi:10.2514/3.22780
- Rizk, N. K., and Lefebvre, A. H. (1982). Spray characteristics of simplex swirl atomizers. (United States). Available at: <https://www.osti.gov/biblio/6169379>.
- Sivakumar, D., Vankeswaram, S. K., Sakthikumar, R., and Raghunandan, B. N. (2015). Analysis on the atomization characteristics of aviation biofuel discharging from simplex swirl atomizer. *Int. J. Multiph. Flow* 72, 88–96. doi:10.1016/j.ijmultiphaseflow.2015.02.009
- Sivakumar, D., Vankeswaram, S. K., Sakthikumar, R., Raghunandan, B. N., Hu, J. T. C., Sinha, A. K., et al. (2016). An experimental study on jatropa-derived alternative aviation fuel sprays from simplex swirl atomizer. *Fuel* 179, 36–44. doi:10.1016/j.fuel.2016.03.050
- Wang, X. F., and Lefebvre, A. H. (1987). Mean drop sizes from pressure-swirl nozzles. *J. Propuls. Power* 3, 11–18. doi:10.2514/3.22946
- Yang, X., Guo, F., Xue, S., and Wang, X. (2016). Carbon distribution of algae-based alternative aviation fuel obtained by different pathways. *Renew. Sustain. Energy Rev.* 54, 1129–1147. doi:10.1016/j.rser.2015.10.045
- Zhou, G., Zhou, J., Fang, Y., and Yang, X. (2019). Properties effect of blending fischer-tropsch aviation fuel on spray performances. *Energy* 179, 1082–1093. doi:10.1016/j.energy.2019.04.157

Funding

This study was supported by the National Key Research and Development Program-China (2018YFB1501505).

Conflict of interest

The authors declare that the research was conducted in the absence of any commercial or financial relationships that could be construed as a potential conflict of interest.

Publisher's note

All claims expressed in this article are solely those of the authors and do not necessarily represent those of their affiliated organizations, or those of the publisher, the editors, and the reviewers. Any product that may be evaluated in this article, or claim that may be made by its manufacturer, is not guaranteed or endorsed by the publisher.

Supplementary material

The Supplementary Material for this article can be found online at: <https://www.frontiersin.org/articles/10.3389/fenrg.2022.944668/full#supplementary-material>